博士論文（要約）

Relative Navigation and Guidance via Direction-Of-Arrival Estimation Method in Deep Space

(Direction-Of-Arrival 推定手法を用いた 深宇宙における相対航法および誘導)

藤田雅大/Masahiro Fujita

Department of Aeronautics and Astronautics
The University of Tokyo

A thesis submitted for the degree of
Doctor of Philosophy

Abstract

Future deep space exploration is expected to be dominated by cooperative missions involving multiple spacecraft, which may include formation flights and rendezvous docking missions. Among these, missions using a large number of ultra-compact probes can enable exploration of target bodies that have been difficult to explore in the past. Autonomous relative navigation and guidance technology is a key technology for realizing missions using multiple ultra-compact probes. Navigation sensors such as cameras and LiDAR are effective when the relative distance between spacecraft is short. Several autonomous navigation and guidance methods using these sensors have been actively studied and demonstrated in orbit. However, there have been few studies conducted on navigation sensors that can be used at medium distances, ranging from tens to hundreds of kilometers.

Therefore, this thesis proposes an autonomous navigation guidance method that uses only angle information estimated by direction of arrival (DOA) estimation method using array antennas. An observer spacecraft receives radio signals emitted by a target spacecraft using an array antenna. The DOA estimation method is applied to the received signals to determine the direction of the target. Navigation and guidance is then performed based on the angle information.

The purpose of this thesis is to establish the autonomous relative navigation and guidance method using the DOA estimation method for middle-range targets. This thesis also demonstrates a solution to a mission with a large number of ultra-compact probes.

This thesis first compares, organizes, and evaluates the array antennas and the DOA estimation algorithms proposed so far using numerical simulations.

Additionally, DOA estimation experiments are conducted using an array antenna and a signal processing system to demonstrate the feasibility of a spacecraft onboard navigation sensor.

Then, the requirements for applying the DOA estimation system to navigation and guidance are summarized. This thesis proposes three methods to meet the requirements, and verifies their effectiveness. The methods are: 1) a high-resolution array and low-cost estimation algorithm, 2) an optimum array design method, and 3) a combined system with a communication system. They are applicable not only for spacecraft navigation and guidance but also for general purposes.

Next, navigation and guidance are discussed. The DOA estimation only provides information about the direction of the radio source (the target spacecraft). Therefore, the features of navigation and guidance using only angle information are presented. Based on the features, an autonomous navigation and guidance algorithm that can be processed on-board is proposed and verified through numerical simulations.

The DOA estimation method and the angles-only navigation and guidance are combined to establish the navigation and guidance using DOA estimation method. First, through covariance analysis, the relations between array antennas, DOA estimation accuracy, and navigation and guidance accuracy are analytically clarified. It is demonstrated that DOA estimation is sufficient for navigation and guidance. Then, A series of steps in the design of the DOA estimation system and the operation of navigation and guidance are then presented.

Finally, a mission study is conducted. The numerical simulations demonstrate that the proposed navigation and guidance method using DOA estimation is feasible for a sample return mission with ultra-compact probes.

Acknowledgements

本論文執筆にあたって，JAXA 宇宙科学研究所の方々を始め，大変多くの方々にお世話になりました．この場を借りて，感謝の意をお伝えいたします．

はじめに，大学院博士課程 3 年間において，親身にご指導を賜りました，津田雄一教授に心より感謝申し上げます．本研究に関するご指導やご助言を賜っただけでなく，研究者としての，研究に対する考え方や心構えなど，大切なことを数多く教えていただきました．研究相談の際には，私がこれまでにあまり持ていなかった，学術的な視点の重要性を示してくださり，本研究をより意義深いものにすることができました．また，はやぶさ 2 のプロジェクトマネージャーとしてのお立場からの知見も豊富であり，本研究が学術的に価値があるだけでなく，実ミッションに即した研究とすることができました．

森治教授には，ソーラー電力セイルプロジェクト，トランスフォーマーミッション，HELIOS・HELIOS-R，輪講，さらには普段の研究生活において，大変お世話になりました．また，本研究の方向性や意義づけに関しても，親身に，様々なご助言を頂きました．大変感謝しております．

佐伯孝尚助教には，STARMINE ミッションの検討などでお世話になりました．その中で，はやぶさ 2 のプロジェクトエンジニアとしてのお立場から，様々な知見をいただきました．この検討の中で示していただいた知見は，今後エンジニアとして働いていく中で，大変参考になるものと考えております．また，飲み会の際に度々お話になっていた，宇宙研・川口研・はやぶさ 2 の裏話など，大変興味深くお聞きしていました．

岩田隆浩准教授には，本研究の副査を務めていただいただけでなく，以前から分野外の研究者としての立場から，本研究に関するご助言をいただきました．その中で，新しい視点で本研究を見つめなおすことができ，大変感謝しております．

JAXA プロジェクト研究員の杉原アフマッド清志さん，久保勇貴さん，東京大学の松下将典さん，九州大学の高尾勇輝助教には，ソーラー電力セイルプロジェクトや HELIOS・HELIOS-R，研究相談などで大変お世話になりました．また，研究生活に関しても貴重なアドバイスをいただきました．私にとって一番身近な研究者として，大変尊敬しております．杉原さんには，本研究における DOA 推定実験でのハードウェア・ソフトウェアの製作，実験の実施に際し，多大な支援をいただきました．電波に関する知識も豊富で，多くのことを学ばせていただきました．久保さんには，旧川口研時代から，研究やスラスタ関係の作業などで大変お世話になりました．同じ部屋ということもあり，些細なことであっても親身に相談に乗っていただき，感謝しております．松下さんには，HELIOS・HELIOS-R で大変お世話になりました．ミッション全体を取りまとめられておられる中で，私が担当していた熱系にもこまめに目をかけてくださり，大変感謝しております．プロジェクトマネジメントの在り方を学ばせていただきました．高尾さんには，研究や HELIOS・HELIOS-R で大変お世話になりました．特に初めての熱試験では多大なご迷惑をおかけしてしまったと思いますが，親身に助言をしてくださったおかげで，試験準備・管理のやり方を学ぶことができました．大変感謝しております．

秘書の木下美夏さんにも，普段の研究生活の様々な場面で，度々多大なるご支援を賜りました．些細な相談にも乗ってくださり，大変感謝しております．

博士学生の臼杵智章さんと吉川健人さんには，プロジェクトや研究のみならず，普段の生活でも多くの場面で非常に密な支援をして頂きました．また，JAXA 職員でもいらっしゃるお立場から，実ミッションに即した的確なアドバイスもいただき，大変参考になりました．

研究室同期の楠本哲也さんと山川真以子さんは，ともに博士号取得を目指す中で切磋琢磨し，大きく成長することができました．私は宇宙研を離れることになりますが，これからも仕事・プライベート関係なくよろしくお願いいたします．

そして後輩の大木春仁さん，中川雄登さん，西村尚さん，保田瞬さん，大月幸穂さん，鶴谷柊朔さん，中川果帆さん，芝田朋世さん，米田大晟さんには，プロジェクトや研究，そして普段の研究生活において大変多くの支援をいただきました．研究を進める中で辛い場面もありましたが，皆さんの存在が大きな心の支えでした．

先生方や研究室の皆様がいなければ，本研究を遂行することはできませんでした. 改めて皆様に深く御礼申し上げます.

卒業後は宇宙研を離れることになりますが，引き続き宇宙業界におりますので，度々お世話になることと思います．いつか皆様とともに，再びおもしろい宇宙ミッションを作っていくことができることを願っております.

そして最後に, これまでの学生生活を支えてくれた家族に感謝いたします．長い学生生活の中で，経済的負担や精神的負担を強いてしまったことと思います．それでも，私の夢の実現が一番だと，多くの支援を賜り，大変感謝しております.

2023 年 12 月 1 日
藤田　雅大

Contents

List of Figures

List of Tables

Chapter 1

Introduction

1.1 Background

1.1.1 Missions Using Multiple Ultra-compact Probes

Cooperative missions using multiple spacecraft will be important for future deep space exploration. According to the Japan's International Space Exploration Scenarios, such as sample return missions and resupply to deep space habitat modules are listed as important items [1]. For instance, JAXA is currently planning the next generation small body sample return mission (NGSR) [3]. In addition, missions that require control of relative position and velocity among spacecraft, such as the satellite interferometer mission using formation flight [4][5], are also attracting attention.

These are the global trends, not only in Japan but also in the United States, Europe, and other regions[6][7][8][9]. For example, NASA is planning the Mars sample return mission consisting of multiple vehicles[7].

The advantages of cooperative missions with multiple spacecraft are described below.

- Robust missions can be realized by dividing the spacecraft functions.
- The risk of losing whole spacecraft system can be reduced by assigning high-risk tasks, such as sample collection, to another small spacecraft.
- Re-supply enables longer mission duration.
- High-resolution and high-precision observations can be made by eliminating physical constraints on sensors (e.g. interferometers).

Here, JAXA's NGSR is discussed as a specific mission. This mission is positioned as the successor to Hayabusa2 [10], which successfully returned samples from the asteroid Ryugu, and Martian Moons eXploration (MMX) [11], which aims to the sample return from the Martian moon Phobos. A multi-spacecraft configuration is being considered for this mission. The configuration includes a parent spacecraft that will make round-trips between Earth and the target asteroid, a child spacecraft that will touch down on the asteroid and collect samples, and ultra-compact probes mounted on the parent spacecraft.

Figure 1.1 shows the overview of the sample collection by the ultra-compact probes. The probes separate from the parent, land on the target body, collect samples, and then depart. The parent then performs rendezvous with some of the probes and retrieves the samples.

Although NGSR will carry only one probe, a new type of exploration can be created if a large number of such probes are used. The mission concept involves deploying a significant number of low-functioning probes to perform various tasks and retrieving them as necessary. The idea is that not all of the probes need to function, but only some of them should. This makes it possible to tolerate failures and to explore high-risk celestial bodies and sites that have been difficult to explore in the past. Although various studies have been conducted [12], all of them are still in the conceptual stage and have not yet been demonstrated. NGSR aims to demonstrate the technologies for such a mission.

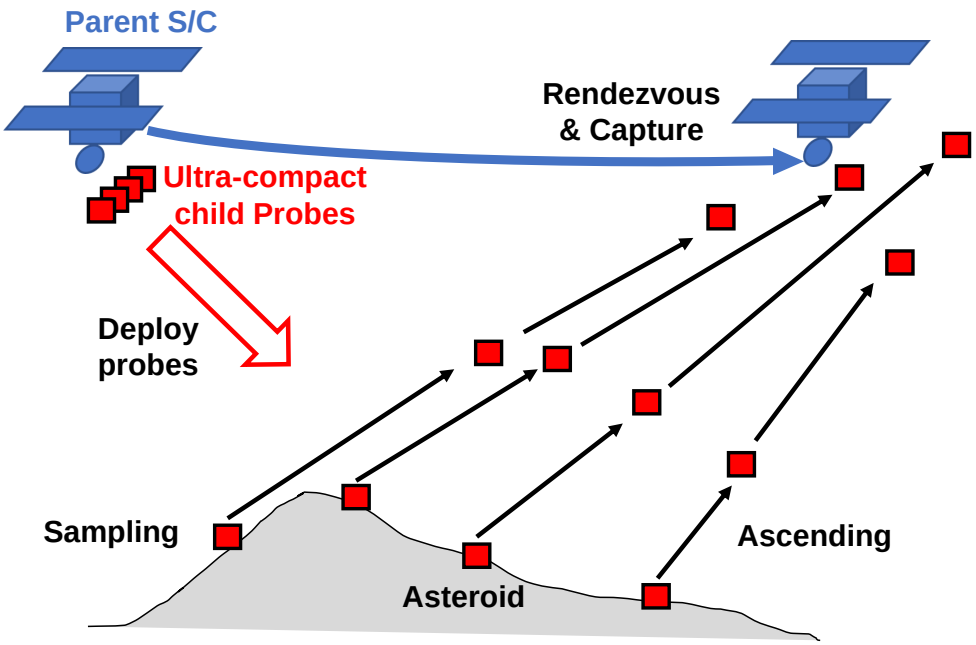

Fig. 1.1: Image of the sample collection by the ultra-compact probes.

To achieve missions with multiple ultra-compact probes, it is important to have low-resource relative navigation and guidance technology, as well as the ability to simultaneously track multiple targets.

1.1.2 Relative Navigation and Guidance for Mid-range Targets

Sensors and methodologies used in relative navigation and guidance can be classified according to the relative distance between spacecraft. Table 1.1 presents the typical navigation sensors, and Fig. 1.2 illustrates the classification of relative navigation sensors according to relative distance.

For long-range targets with a relative distance of several hundred kilometers or more, absolute navigation using range and range rate (RARR) and delta-differential one-way range (DDOR) with ground stations are employed instead of relative navigation. Orbit determination (navigation) and orbit planning (guidance) are typically conducted offline at ground stations. While the accuracy of RARR and DDOR is high, it is not suitable for short-range navigation and guidance due to the need for communication with ground stations and offline processing.

Various navigation sensors have been developed for short-range targets with a relative distance of less than a few kilometers (Table 1.1). Cameras can measure direction, distance, and attitude depending on the distance. Cameras are relatively inexpensive, small, and simple. However, their performance is limited by optical conditions, such as inappropriate surface optical properties of the target or inapplicability when the target is in the shade, etc. Light detection and ranging (LiDAR) is a one-dimensional distance measurement device, which is used by various missions, including Hayabusa2 [13]. Additionally, Japan and other countries are developing 3D-LiDAR, a sensor capable of estimating the 3D position of a target [14][15]. Millimeter wave radar (MWR), such as frequency modulated continuous wave (FMCW) radar used in automobiles, is also effective as a distance measurement sensor, although its use is limited to the vicinity of several hundred meters or less. Navigation and guidance is performed online by combining information obtained from the various sensors mentioned above. In the vicinity of Earth, external reference information such as Global Navigation Satellite System (GNSS) and the two-line element (TLE) may also be used for the robust navigation. There were lots of experiments in orbit such as Engineering Test Satellite-VII (ETS-VII) [?][?], Prototype Research Instruments and Space Mission Technology Advancement (PRISMA) [?][?][?], End-of-Life

Services by Astroscale - demonstration (ELSA-d) [**?**] and so on.

For middle-range targets (relative distance: several hundred meters to several hundred kilometers), the effective navigation sensors are Proximity Communication System (PROX) [16] and cameras. PROX is installed in the Japanese Experiment Module (JEM) on the International Space Station (ISS) and transmits GNSS data for navigation to the H-II Transfer Vehicle (HTV). However, PROX requires transponders for both the target spacecraft and observer spacecraft, which adds complexity to the system. It is only available in the vicinity of Earth. Thus, the available navigation sensors are limited to cameras. In NASA's Mars sample return mission, the Earth return vehicle would perform several maneuvers to navigate into the vicinity of the orbiting sample (OS) using the onboard camera [7]. However, as mentioned above, cameras are severely limited by the optical conditions, and the amount of light captured by the cameras decreases inversely with the square of the distance. Additionally, a camera can only provide angular information at medium distances, requiring special navigation and guidance techniques (see Chapter 5 for details). For near-Earth missions (regions closer than Moon), the combination of the external reference information such as GNSS and TLE is effective [**?**][**?**][**?**][17][18][**?**]. However, in deep space beyond Moon, such external reference information is basically not available. Therefore, it is necessary to develop a navigation sensor and a navigation and guidance method that can be used for the middle-range target regardless of the optical conditions.

Tab. 1.1: Representative navigation sensors [1].

Navigation sensor	Applicable range	Range	Angle	Attitude	Accuracy
1D-LiDAR	$<$ 10s of km	+	-	-	$\pm$10m
PROX	$<$ 100s of km	+	-	-	$<$ 10m
Camera	$<$ 100s of km	-	+	-	$<$ 0.1deg. (angle)
Camera	$<$ 100s of m	+	+	-	10% (range)
Camera	$<$ 10s of m	+	+	+	A few deg. (attitude)
3D-LiDAR	$<$ A few km	+	+	+	A few cm & $<$0.1 deg.
MWR	$<$ 100 m	+	-	-	0.1-0.4m @ 20-160m

1.1.3 Estimation of Direction of Arrivals of Radio Waves

One of the effective methods for the middle-range navigation is to estimate the direction of arrival of radio waves emitted by the targets. The advantages of using the radio waves are as follows:

- Angle information can be obtained for the middle-range targets where cameras are not available.
- Available in the proximity regardless of the optical conditions (as a backup of cameras)
- Since the angle information is obtained, it is compatible with the navigation and guidance method that uses only angle information, which has been studied in the past.

There are various possible methods for estimating the direction of arrival of radio waves. For example, the following method can be considered: a gimbal is used to mechanically move the antenna to perform a spatial search, and the direction of maximum received power is considered to be the direction of arrival. Figure 1.3 shows the middle gain antenna (MGA) onboard Hayabusa2. The antenna is equipped with a gimbal that has two axes of azimuth and elevation, allowing it to be mechanically pointed in the specified direction. Although this two-axis gimbal is not be used to estimate the direction of arrival of radio waves in Hayabusa2, it can be used to estimate the direction of a radio source. However, this method has the following disadvantages.

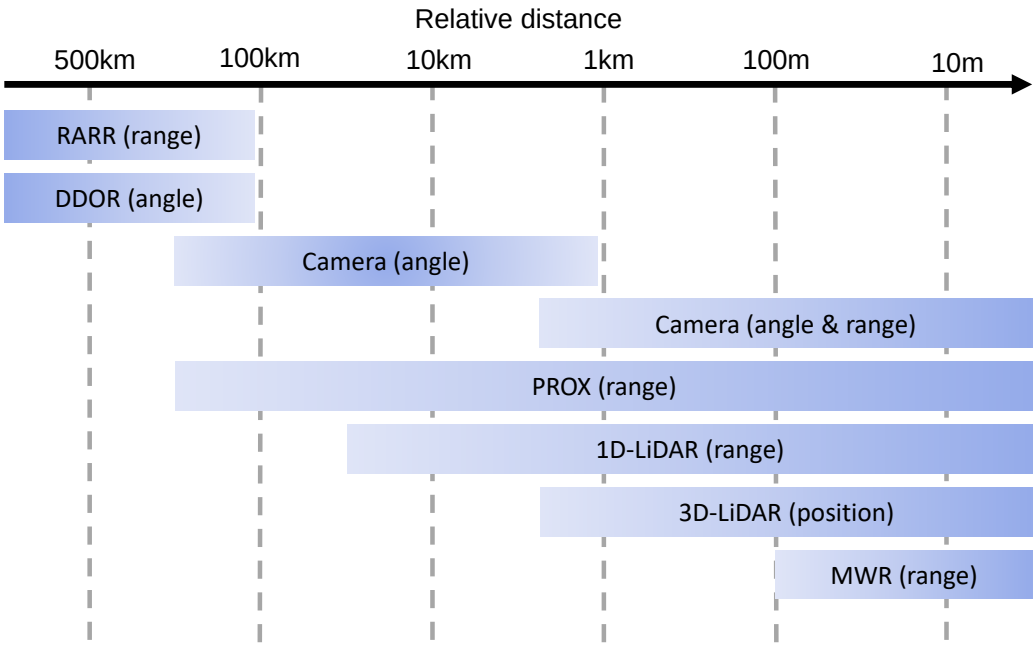

Fig. 1.2: Sensors (methodologies) v.s. relative distance [1].

- A gimbal driving mechanism is required.
- Spatial search is time-consuming.
- Low resolution because the resolution depends on the beam width of the antenna.

Because of the above disadvantages, it is not realistic to use this method.

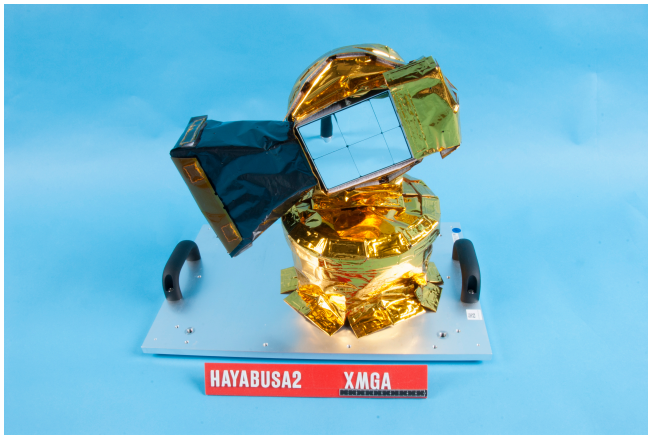

Fig. 1.3: MGA of Hayabusa2. (C)JAXA

Therefore, this thesis proposes a method that utilizes array antennas. An array antenna consists of multiple antenna elements arranged on an antenna board as shown in Fig. 1.4. The array antenna receives radio waves and measures the phase difference between the elements. This phase difference information is used to estimate the direction of arrival of a radio wave. This method is simply called "Direction-Of-Arrival (DOA) estimation method". The following are some of the advantages of DOA estimation method.

- No driving mechanism is required.

- No spatial search is required, or it can be done electrically, so the estimation time is short.
- High-resolution and high-precision estimation that exceeds the beam width limit is possible.
- Simultaneous angle measurement is possible.

There have been many studies on DOA estimation methods. However, most of them are simulation-based studies for the ground applications such as radar and mobile communications. Therefore, there are various issues to be solved in order to apply DOA estimation method as an angle measurement method for autonomous relative navigation and guidance in deep space.

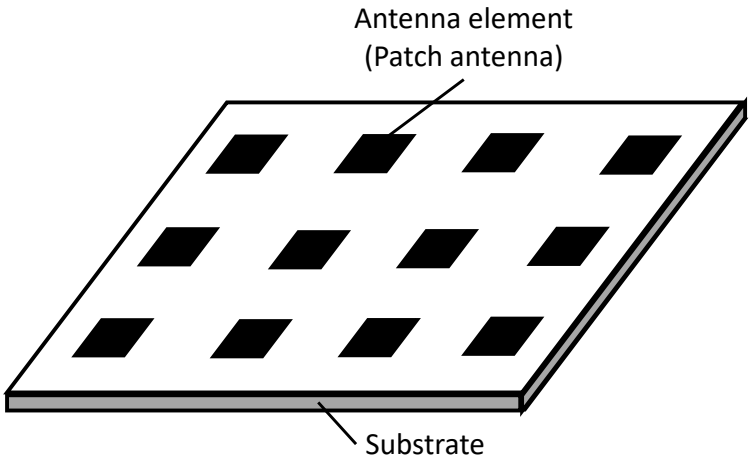

Fig. 1.4: Array antenna.

1.1.4 Relative Navigation and Guidance via DOA Estimation Method

This thesis proposes a method for relative navigation and guidance using DOA estimation method. A spacecraft that emits radio waves and that is the target of navigation and guidance is called a "Target". On the other hand, a spacecraft that receives radio waves from a Target and provides navigation and guidance is referred to as an "Observer". An overview of the proposed method is shown in Figure 1.5. The following outlines the procedures.

- Target emits radio waves using omni-directional antennas.
- Observer receives the radio wave using its own array antenna and estimates the DOAs of the signals.
- Observer estimates Target's relative orbit (relative position and velocity) using only the DOA information (navigation).
- Observer performs maneuvers as necessary (guidance).

The proposed method enables relative navigation and guidance in the medium distances (several kilometers to several hundred kilometers), regardless of optical conditions. The navigation and guidance in this method (Chapter 5) is also applicable to camera-based navigation and guidance, so the transition to camera navigation is smooth.

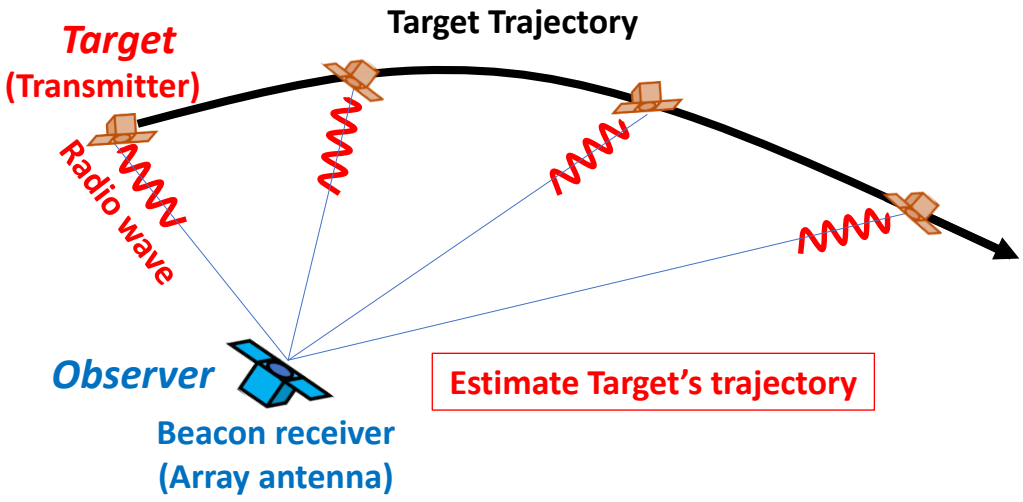

Fig. 1.5: Overview of the proposed method.

1.2 Purpose and Contributions

Purpose

The purpose of this thesis is to establish an autonomous relative navigation and guidance method using the DOA estimation method for middle-range targets with a relative distance of several hundred meters to several hundred kilometers. This thesis demonstrates a solution to a mission with a large number of ultra-compact probes.

Contributions

The contributions of this thesis are presented. One is that a solution for a mission with a large number of ultra-compact probes is presented. A concrete solution to the mission, which was previously only at the conceptual level, is shown from the perspective of relative navigation and guidance.

In addition, the DOA estimation method, which has been mainly used on the ground, is extended to the use as a navigation sensor in deep space. A low-resource array antenna and DOA estimation algorithm are implemented for use in space, as described in Chapter 4. The method is also applicable to the ground-based applications and has a variety of possible uses.

The navigation and guidance method using only angular information, which has been intended for cameras, is also extended to array antennas (extension of the academic domain). This allow the same navigation and guidance law to be applied while switching between different navigation sensors (cameras and array antennas) from the near to mid-range regions. Chapter 5 presents a navigation and guidance method with low computational cost and proposes a solution for on-board navigation and guidance.

1.3 Thesis Overview

Figure 1.6 summarizes the thesis overview. The proposed method for relative navigation and guidance consists of two parts: direction estimation of the radio source (target) using the DOA estimation method and relative navigation and guidance using only angle information.

In Chapter 2, the directional estimation of radio sources using the DOA estimation method is described. The basic principles of the DOA estimation method, estimation algorithms, and array antennas are summarized, and numerical simulations are used to compare them. The characteristics of the DOA estimation methods are evaluated.

In Chapter 3, the DOA estimation experiments conducted by an array antenna and signal processing system are discussed, and clarify the requirements for the installing the DOA estimation system on a spacecraft.

Chapter 4 summarizes the requirements for installing a DOA estimation system on a spacecraft based on the discussions in Chapters 2 and 3. Three methods are proposed and verified to meet those requirements.

Chapter 5 describes relative navigation and guidance using only angle information. When only angle information is available as an observable quantity, an appropriate maneuver can improve observability. In this chapter, the maneuvers that maximize observability are examined based on previous studies. Based on the results, a new relative navigation and guidance method that maximizes observability while minimizing the amount of fuel consumption with low computational cost is proposed and evaluated.

In Chapter 6, the relative navigation and guidance using DOA estimation method is established based on the results of the studies in Chapters 2 to 5.

In Chapter 7, a mission study is conducted to validate the methodology established in Chapter 6.

In conclusion, Chapter 8 discusses the summary and the contributions of this thesis.

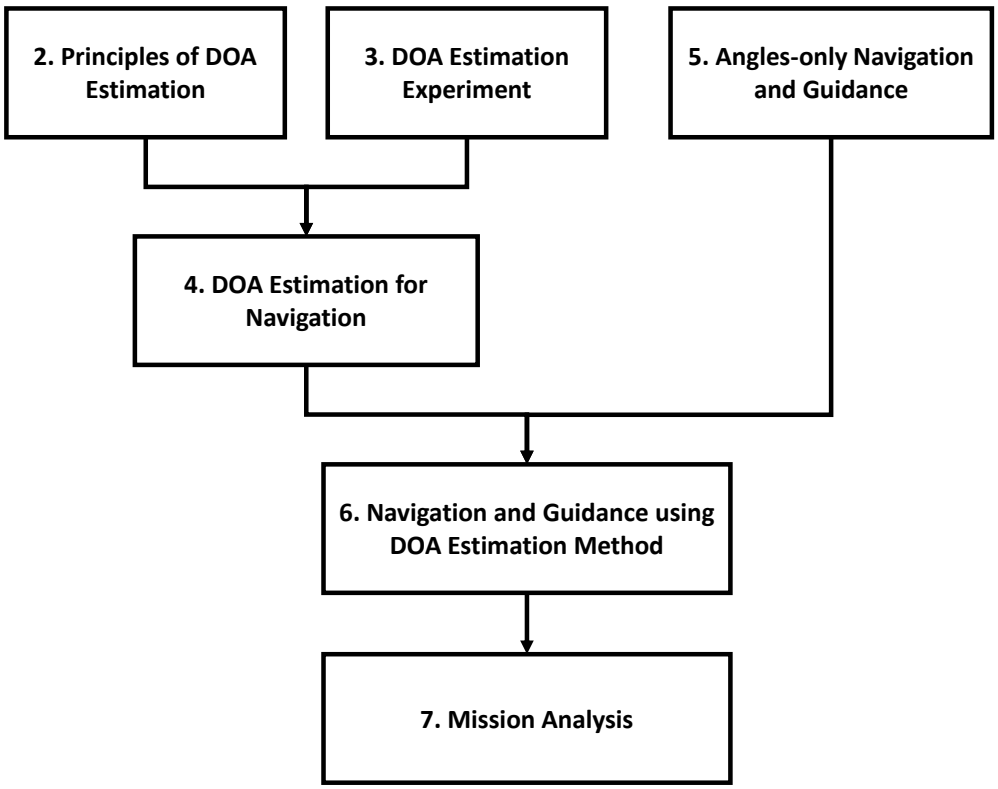

Fig. 1.6: Thesis overview.

Chapter 2

Principles of DOA Estimation

2.1 Problem Formulation

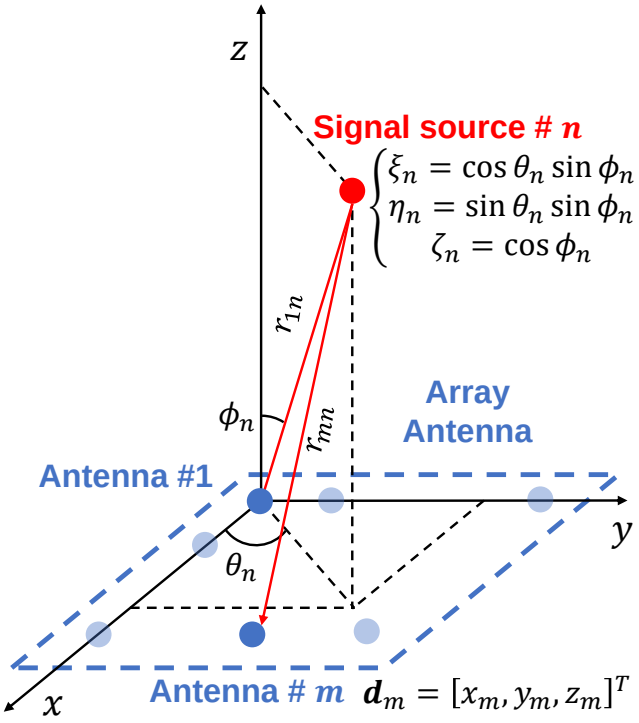

Fig. 2.1: Geometrical relations between the antenna elements and the signal sources.

Suppose that an array antenna with M elements receives signals from N independent signal sources. Figure 2.1 shows the geometric relations between the array antenna and the signal sources. The reference point of the coordinate is fixed at the 1-st antenna element. When the n-th signal source is located at a distance of r_{1n} and its azimuth and zenith are θ_n and ϕ_n, the position vector of the source $\boldsymbol{r}_{1n}$ can be expressed as follows:

$$\boldsymbol{r}_{1n} = \begin{bmatrix} r_{1n}\cos\theta_n \sin\phi_n \\ r_{1n}\sin\theta_n \sin\phi_n \\ r_{1n}\cos\phi_n \end{bmatrix} \tag{2.1}$$

If the m-th antenna element is located at the position $\boldsymbol{d}_m \equiv [x_m, y_m, z_m]^T$, the position of the n-th source relative to the m-th element $\boldsymbol{r}_{mn}$ can be expressed as:

$$\boldsymbol{r}_{mn} = \boldsymbol{r}_{1n} - \boldsymbol{d}_m = \begin{bmatrix} r_{1n}\cos\theta_n \sin\phi_n - x_m \\ r_{1n}\sin\theta_n \sin\phi_n - y_m \\ r_{1n}\cos\phi_n - z_m \end{bmatrix} \tag{2.2}$$

Therefore, the difference of the propagation path between the reference point (1-th element) and the m-th element is calculated:

$$\Delta r_{mn} = r_{mn} - r_{1n} \tag{2.3}$$

When the distance between the antenna and signal source is much larger than the array size, Δr_{mn} can be approximated:

$$\begin{aligned} \Delta r_{mn} &\approx x_m \cos\theta_n \sin\phi_n + y_m \cos\theta_n \sin\phi_n + z_m \cos\phi_n \\ &= \boldsymbol{d}_m^T \boldsymbol{L}(\theta_n, \phi_n) \end{aligned} \tag{2.4}$$

where $\boldsymbol{L}(\theta, \phi)$ is the line-of-sight (LOS) vector, defined as:

$$\boldsymbol{L}(\theta, \phi) = \begin{bmatrix} \cos\theta \sin\phi \\ \sin\theta \sin\phi \\ \cos\phi \end{bmatrix} \tag{2.5}$$

Here, a transformation is performed as follows:

$$\begin{cases} \xi = \cos\theta \sin\phi \\ \eta = \sin\theta \sin\phi \end{cases} \tag{2.6}$$

Equation 2.5 can be expressed using Eq.2.6:

$$\boldsymbol{L}(\theta, \phi) = \begin{bmatrix} \xi \\ \eta \\ \sqrt{1 - (\xi^2 + \eta^2)} \end{bmatrix} \equiv \hat{L}(\xi, \eta) \tag{2.7}$$

Thus, the phase difference of the received signal between the 1-st element and m-th element is calculated:

$$\Delta\psi_{mn} = \frac{2\pi}{\lambda}\Delta r_{mn} = \frac{2\pi}{\lambda}\boldsymbol{d}_m^T \boldsymbol{L}(\theta_n, \phi_n) = 2\pi \hat{\boldsymbol{d}}_m^T \hat{\boldsymbol{L}}(\xi_n, \eta_n) \tag{2.8}$$

where λ is the wavelength of the signal and $\hat{\boldsymbol{d}}_m = [u_m, v_m, w_m]^T$ is the position vector normalized by λ. Therefore, Eq. 2.8 is expressed as follows:

$$\Delta\psi_{mn} = \frac{2\pi}{\lambda}\boldsymbol{d}_m^T \boldsymbol{L}(\theta_n, \phi_n) = 2\pi \hat{\boldsymbol{d}}_m^T \hat{\boldsymbol{L}}(\xi_n, \eta_n) = 2\pi \left(u_m \xi_{0n} + v_m \eta_{0n} + w_m \sqrt{1 - (\xi^2 + \eta^2)} \right) \tag{2.9}$$

Now the received signal at the array antenna is considered. Suppose the signal at n-th source is expressed as:

$$s_{n0}(t) = b_{n0} \exp\left[j \left(2\pi f t + \psi_n \right) \right] \tag{2.10}$$

where f is the frequency of the signal, b_{n0} is the signal amplitude, and ψ_n is the signal phase. The signal is propagated and received at the antenna element. The normalized received signal at m-th element as follows:

$$x_{mn}(t) = \exp\left[j \left(2\pi f t + \psi_n + \frac{2\pi}{\lambda} r_{mn} \right) \right] \tag{2.11}$$

x_{mn} can be rearranged using Eqs. (2.2), (2.4), and (2.8) :

$$x_{mn}(t) = \exp\left[j\left(2\pi ft + \Psi_n + 2\pi \hat{\boldsymbol{d}}_m^T \hat{\boldsymbol{L}}(\xi_n, \eta_n)\right)\right] \tag{2.12}$$

$$= f_n(t) a_{mn} \tag{2.13}$$

where

$$\Psi_n = \frac{2\pi}{\lambda} r_{1n} + \psi_n \tag{2.14}$$

$$f_n(t) = \exp\left[j\left(2\pi ft + \Psi_n\right)\right] \tag{2.15}$$

$$a_{mn} = \exp\left[j\left(2\pi \hat{\boldsymbol{d}}_m^T \hat{\boldsymbol{L}}(\xi_n, \eta_n)\right)\right] \tag{2.16}$$

Therefore, all of the received signals at the m-th antenna element $x_m(t)$ can be expressed as:

$$x_m(t) = \sum_{n=1}^{N} x_{mn}(t) + n_m(t) \tag{2.17}$$

where $n_m(t)$ is the internal noise. The received signal at all of the elements is expressed as follows:

$$\boldsymbol{X}(t) = \begin{bmatrix} \sum_{n=1}^{N} x_{1n}(t) + n_1(t) \\ \vdots \\ \sum_{n=1}^{N} x_{Mn}(t) + n_M(t) \end{bmatrix} = A\boldsymbol{F}(t) + \boldsymbol{\Sigma}(t) \tag{2.18}$$

where

$$\boldsymbol{X}(t) = \begin{bmatrix} x_1(t), & \cdots, & x_M(t) \end{bmatrix}^T \tag{2.19}$$

$$A = \begin{bmatrix} \boldsymbol{a}_1, & \cdots, & \boldsymbol{a}_N \end{bmatrix} \tag{2.20}$$

$$\boldsymbol{a}_n = \begin{bmatrix} a_{1n}, & \cdots, & a_{mn} \end{bmatrix}^T \tag{2.21}$$

$$\boldsymbol{F}(t) = \begin{bmatrix} f_1(t), & \cdots, & f_N(t) \end{bmatrix}^T \tag{2.22}$$

$$\boldsymbol{\Sigma}(t) = \begin{bmatrix} n_1(t), & \cdots, & n_M(t) \end{bmatrix}^T \tag{2.23}$$

where A is called the direction matrix and $\boldsymbol{F}(t)$ is the signal source vector. The cross-correlation matrix is then calculated as follows:

$$R_{xx} = E[\boldsymbol{X}(t)\boldsymbol{X}^H(t)] = ASA^H + P_{noise} I \tag{2.24}$$

where $E[\cdot]$ is the expectation (ensemble average), $(\cdot)^H$ is the complex conjugate transpose of the matrix, P_{noise} is the power of the internal noise, I is the identity matrix and S is the cross-correlation matrix of the signals and is expressed as:

$$S = \begin{bmatrix} E[|f_1(t)|^2] & E[f_1(t)f_2^*(t)] & \cdots & E[f_1(t)f_N^*(t)] \\ E[f_2(t)f_1^*(t)] & E[|f_2(t)|^2] & \cdots & E[f_2(t)f_N^*(t)] \\ \vdots & \vdots & \ddots & \vdots \\ E[f_N(t)f_1^*(t)] & E[f_N(t)f_2^*(t)] & \cdots & E[|f_N(t)|^2] \end{bmatrix} \tag{2.25}$$

If the signals are uncorrelated with each other, S is the diagonal matrix:

$$S = \mathrm{diag}\left[P_1, \quad \cdots, \quad P_N\right] \tag{2.26}$$

where P_n is the n-th signal power. Because the signal can be considered ergodic, R_{xx} can be approximated by taking multiple snapshots of the received signal and averaging them over time.

$$R_{xx} \approx \frac{1}{L}\sum_{i=1}^{L} \boldsymbol{X}(t)\boldsymbol{X}^H(t) \tag{2.27}$$

where L is the number of snapshots (samples). The direction of the radio source is estimated using the cross-correlation matrix in the DOA estimation method. The algorithms are introduced in the next section.

2.2 DOA Estimation Algorithm

DOA estimation method uses the cross-correlation matrix R_{xx} obtained by the array antennas to estimate the direction of the signal source. Various algorithms have been proposed and some of the representative ones are shown in Table. 2.1.

Fast Fourie transformation (FFT) obtains the intensity distribution of radio sources by performing a two-dimensional Fourier transform on the cross-correlation (visibility).

Beamformer scans the main beam of an array antenna in all directions to find the direction where the output power of the array is larger [19].

Both FFT and Beamformer have low resolution due to the beam width of the array antennas. Therefore, a high resolution method using eigenvalue decomposition of cross-correlation has been proposed. The eigenvalue decomposition of cross-correlation matrix separates the Hermite space in M dimension into a signal subspace and a noise subspace. Depending on which subspace is focused on, two main methods are proposed: MUSIC and ESPRIT.

MUSIC (MUltiple SIgnal Classification) [20] performs DOA estimation by focusing on the noise subspace. The MUSIC spectrum is calculated and its peaks are regarded as the DOAs. Since spectral search is required, the computational cost is high. It can be applied to any array configurations.

ESPRIT (Estimation of Signal parameters via Rotational Invariance Techniques) [21][22][23] performs DOA estimation by focusing on the signal subspace. The DOAs are calculated without the spectral search. Since spectral search is not required, the computational cost is low. On the other hand, the array configuration is limited to uniform or "hole-free" arrays (explained in 2.3).

Each of the algorithms is explained more in detail in Appendix. D.

Tab. 2.1: Summary of the DOA estimation algorithms.

Algorithm	Array antenna	Principles	Estimation accuracy
FFT	Arbitrary	Fourier transformation	Low
Beamformer	Arbitrary	Spatial search	Low
MUSIC	Arbitrary	Eigendecomposition, Spatial search	High
ESPRIT	Hole-free	Eigendecomposition	High

2.3 Array Antenna for DOA Estimation

An array antenna consists of multiple antenna elements arranged on a flat substrate, as shown in Fig. 1.4. Any type of antenna element can be used, but patch antennas are generally used for compactness. For more information on how to design antenna patches and the substrate, see [2].

The accuracy and resolution of DOA estimation methods depend on the arrangement of array antenna elements as well as on the estimation algorithm. The most basic arrays are uniformly arranged arrays such as a uniform linear array (ULA) and a uniform rectangle array (URA). The element spacing is often set to half the wavelength of the center frequency of the received signal (i.e. $\lambda/2$). Fig. 2.2 shows an example of URAs.

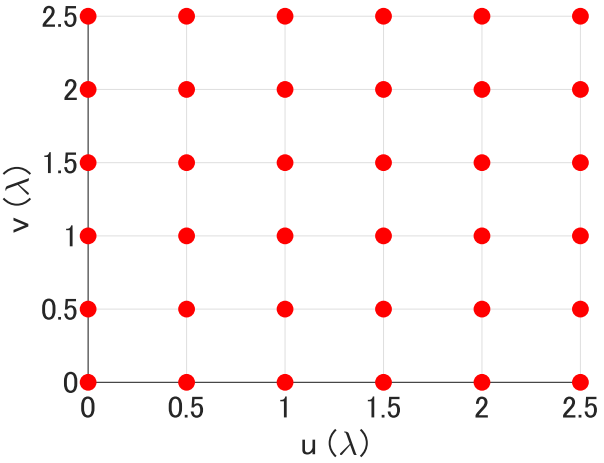

Fig. 2.2: Example of URA (36 elements).

There are three main considerations when designing array antennas: maximum baseline length, element spacing and mutual coupling effects.

In general, angular resolution and maximum baseline length (maximum distance among the elements) have the following relationship:

$$\theta_{res} \sim \frac{\lambda}{D_{max}} \tag{2.28}$$

where θ_{res} is the angular resolution and D_{max} is the maximum baseline length. To achieve high resolution, a long maximum baseline length is required.

If the element spacing is larger than $\lambda/2$, ambiguity appears in addition to the true DOA. Such ambiguity does not appear when the element spacing is less than $\lambda/2$. This principle is explained more in detail in Appendix A.

On the other hand, as the element spacing decreases, the influence of the mutual coupling effect increases. The mutual coupling effect is an effect in which the output current of the antennas differ from the theoretical values when the antennas are close to each other, due to the mutual exchange of energy by rescatter [24][25][26][27][28][29][30][31][32][2]. It depends on the antenna characteristics and the antenna spacing, and the closer the antenna spacing, the greater the effect. Various methods have been proposed to remove mutual coupling effects. One of the methods is described in Appendix B, which is briefly described as a method based on the actual and theoretical cross-correlations of array antennas obtained by the least squares method. Another method is to obtain the mutual coupling matrix by measuring the impedance of the antennas.

URAs and ULAs are the most basic ambiguity-free array antennas, but the elements are densely spaced at half-wavelength intervals and are very sensitive to the mutual coupling effects. In addition, it is difficult to increase the maximum baseline length, making it impossible to achieve high resolution with small number of elements.

Therefore, an array antenna with a sparse element arrangement, called a sparse array, has been developed. The sparse element array reduces the mutual coupling effects and increases the maximum baseline length. Various sparse arrays have been considered, the most effective of which is the "hole-free" array in which the "differential coarrays" are equivalent to URAs. The differential coarray is the virtual array defined by the relative position of the elements. That is, hole-free array means that when the relative position vectors among the elements are plotted, they are uniformly aligned

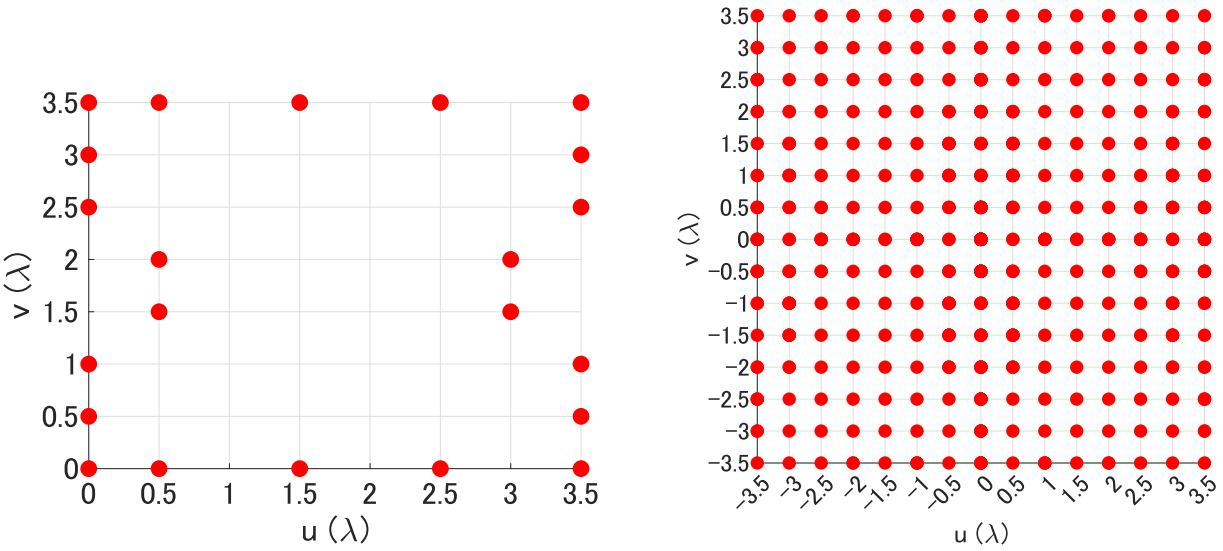

(a) Array configuration.

(b) Differential coarray.

Fig. 2.3: Example of hourglass array (22 elements).

at half-wavelength intervals, as in URA. This prevents the creation of ambiguity. Several kinds of hole-free arrays have been proposed, including open box array (OBA), half open box array (HOBA), HOBA-2, and hourglass arrays[33][34]. Figure 2.3a shows the example of the hourglass array and Fig. 2.3b shows the differential coarray.

2.4 Numerical Simulation

In 2.1, 2.2, and 2.3, the algorithms of the DOA estimation and the array antennas have been described. In this section, some of the arrays and algorithms are compared by numerical simulations to understand their characteristics.

The contents in this chapter is omitted in this version for future publications.

2.5 Summary

The DOA estimation algorithm and the array antenna are described and compared by numerical simulation. Based on the result, the characteristics of the DOA estimation algorithm and array antennas can be summarized as follows.

Array antenna

An array antenna is an antenna that consists of multiple antenna elements on a substrate. The design of array antennas requires the avoidance of ambiguity and mutual coupling effects, as well as an increase in the maximum baseline length. The most basic array configuration is the URA with $\lambda/2$ element spacing. Although it avoids ambiguity, it is susceptible to mutual coupling effects and it is difficult to increase the maximum baseline length, making it difficult to achieve high estimation accuracy and resolution. Hole-free sparse arrays such as HOBA-2 and hourglass array can improve estimation accuracy and resolution by avoiding ambiguity, reducing mutual coupling effects, and increasing the maximum baseline length.

Estimation algorithm

Estimation algorithms are applied to the cross-correlation matrix obtained from the array antennas to perform DOA estimation. Interferometry performs estimation by performing a two-dimensional Fourier transform on the cross-correlation, and Beamformer performs estimation by spatially searching the array beam. Both of these methods have low estimation accuracy and resolution since the resolution is limited by the beamwidth of the array. On the other hand, MUSIC and ESPRIT are methods that perform eigenvalue decomposition of the cross-correlation matrix. By performing eigenvalue decomposition, the Hermite space can be decomposed into a signal subspace and a noise subspace. MUSIC focuses on the noise subspace, calculates the MUSIC spectrum, and performs spatial search for estimation. While it is computationally expensive, it can be applied to arbitrary array configurations. ESPRIT focuses on the signal subspace and performs estimation without spatial search. While the computational cost is low, the arrays are restricted to URA or hole-free arrays.

Table 2.2 shows an example of link budget. If the transmit power is 1 [W], the SNR at 1,000 [km] is -10 [dB]. In other words, the desired signal power is equal to or lower than the internal noise power. However, it can be seen that MUSIC and ESPRIT can measure angles with high accuracy.

Tab. 2.2: Example of link budget analysis.

	Unit				
Center frequency	GHz	8.5	8.5	8.5	8.5
Bandwidth	kHz	10.0	10.0	10.0	10.0
Equivalent Isotropic Radiation Power(EIRP)	dBW	-1.0	-1.0	-1.0	-1.0
Free Space Path Loss (FSPL)	dB	-111.0	-131.0	-151.0	-171.0
Distance	km	1	10	100	1,000
Receive power	dBW	-112.0	-132.0	-152.0	-172.0
Antenna gain (receive)	dBi	2.0	2.0	2.0	2.0
Noise Figure (NF)	dB	4.0	4.0	4.0	4.0
Noise Spectral Density (NSD)	dBHz	-203.8	-203.8	-203.8	-203.8
SNR	dB	49.8	29.8	9.8	-10.2

Chapter 3

DOA Estimation Experiment

In this chapter, the DOA estimation experiment conducted by fabricating array antennas and signal processing systems is described. Experiments on DOA estimation using array antennas have been conducted in the past. On the other hand, experiments using hardware designed to be installed on a spacecraft have not been conducted until now. In this thesis, as a joint experiment with the JAXA Exploration Hub, an array antenna and signal processing systems are constructed. This experiment is conducted to demonstrate that DOA estimation can be performed, and to understand the characteristics of hardware and software for performing DOA estimation in deep space.

Through this experiment, a very compact system that can estimate DOA with an accuracy of 0.005 (in ξ and η) is established.

The contents in this chapter is omitted in this version for future publications.

Chapter 4

DOA Estimation for Navigation

In Chapter 2, the principle of the DOA estimation method and the basics of array antennas are explained and compared with each other based on the numerical simulations. In Chapter 3, the DOA estimation experiment is performed with the DOA estimation system including the compact 16-element HOBA-2 array, and the estimation accuracy are estimated.

In this chapter, the requirements for applying the DOA estimation method to the navigation in deep space missions, and new methods to meet the requirements are proposed.

The contents in this chapter is omitted in this version for future publications.

Chapter 5

Angles-only Navigation and Guidance

This chapter and the subsequent chapters discuss how to perform relative navigation and guidance using the DOA estimation method. Its features include the following:

- Only the angle information of the target obtained by DOA estimation is available.
- Autonomous navigation and guidance is required.

This chapter first summarizes the general characteristics of relative navigation and guidance when only the angle information is observed. Next, based on the characteristics, a new autonomous relative navigation and guidance method are proposed and evaluated.

The contents in this chapter is omitted in this version for future publications.

Chapter 6

Relative Navigation and Guidance via DOA Estimation Method

In Chapters 2 through 4, only the DOA estimation is discussed, and in Chapter 5, only the relative navigation and guidance using angle information is discussed. In this chapter, the previous discussions are integrated and organized, and a navigation and guidance method using DOA estimation method is established.

The contents in this chapter is omitted in this version for future publications.

Chapter 7

Mission Analysis

In this chapter, the proposed navigation and guidance using the DOA estimation method in Chapter 6 is examined using a specific mission as the subject.

As an example of the mission, a sample return mission by the multiple ultra-compact probes is defined. Since the rendezvous and docking phase is of particular interest in this thesis, only the part related to this phase is designed in this chapter.

The contents in this chapter is omitted in this version for future publications.

Chapter 8

Conclusion

This thesis presents a new method for relative navigation and guidance using DOA estimation method, which is effective in the mid- to far-field, and has presented a solution for missions with a large number of ultra-compact probes. In the proposed method, an observer spacecraft receives radio waves emitted by the targets using an array antenna and estimates the direction of arrival of the waves using the DOA estimation method. The obtained DOA information is used to estimate the relative orbits of the targets. The following is a summary of the main results obtained from this thesis.

Chapter 2 presents the fundamental principles of the DOA estimation method, introduces the estimation algorithms and array antennas that have been proposed, and performs numerical simulations to compare their characteristics.

In Chapter 3, an array antenna and signal processing system are constructed, and the DOA estimation experiment was conducted. By taking into account the distance between the transmitter and receiver and the mutual coupling effect, it was found that the DOA could be estimated with an accuracy of about 0.005 (ξ and η).

Chapter 4 presents the requirements for applying DOA estimation to navigation and guidance, based on the studies in Chapters 2 and 3. Three methods to satisfy these requirements are proposed: the distributed arrays and HEMEA, the optimal array design method, and the system combined with a communication system. The method to realize a low-resource and highly accurate DOA estimation system was established.

In Chapter 5, the characteristics of navigation when only angle information is available and the effect of maneuvers on the observability improvement were first presented. Then, the method for autonomous navigation and guidance using only angle information was proposed and verified.

In Chapter 6, the relation between DOA estimation accuracy and navigation and guidance accuracy is estimated. A method for relative navigation and guidance using DOA estimation method was developed and verified.

Chapter 7 presents the results of a mission study that assumed a sample return mission using a large number of ultra-compact probes. The study verified the effectiveness of the relative navigation and guidance using the DOA estimation method.

As previously mentioned, the navigation and guidance using DOA estimation proposed in this thesis can be used in the situations where cameras cannot be used as navigation sensors, and will greatly contribute to multiple spacecraft missions in deep space. The proposed navigation and guidance method in Chapter 5 is also applicable to the camera-based navigation, and contributes significantly to onboard image-based navigation and guidance technology, which has been the focus of attention for some time. The low-resource and high-accuracy DOA estimation system has also been proposed based on the DOA estimation method, which has been mainly used in the ground application. This system is expected to be effective not only in deep space but also in situations where low resources are required. The author believes that the construction of navigation and guidance using DOA estimation will enable a new type of mission using a large number of ultra-compact probes.

Appendix A

Ambiguity

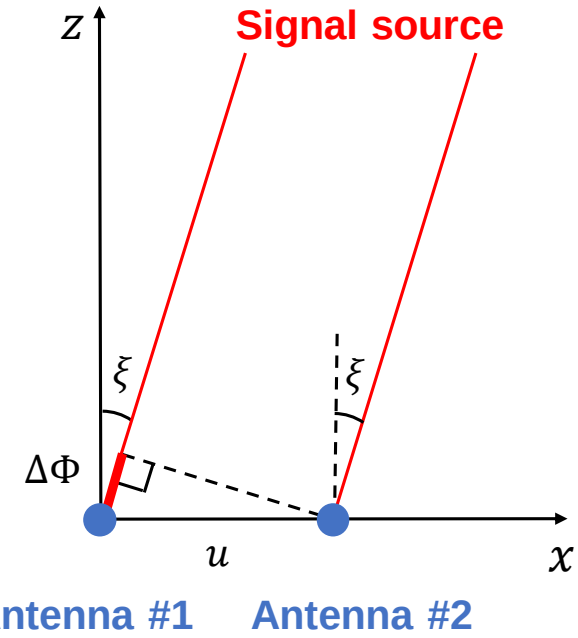

Fig. A.1: Geometric relation of the two-element linear array.

When there is a signal source in the direction $\left[\xi, \eta, \sqrt{1-(\xi^2+\eta^2)}\right]$, the phase difference between two antenna elements with element spacing vector $\boldsymbol{d} = [u, v, w]$ can be expressed as:

$$\Delta\Phi = 2\pi\left(u\xi + v\eta + w\left(\sqrt{1-(\xi^2+\eta^2)}\right)\right) \tag{A.1}$$

If the array is linear and the element spacing vector $\boldsymbol{d}$ is expressed as $\boldsymbol{d} = [u, 0, 0]$ (Fig. A.1), the phase difference is expressed as:

$$\Delta\Phi = 2\pi u\xi \qquad (-1 \leq \xi \leq 1) \tag{A.2}$$

To eliminate ambiguity, it is necessary and sufficient that no ξ' exists that satisfies

$$2\pi u\xi = 2\pi u\xi' + 2\pi n \Leftrightarrow \xi = \xi' + \frac{n}{u} \qquad (-1 \leq \xi \leq 1) \tag{A.3}$$

where n is a non-zero integer. From Eq. A.3, the following relation can be obtained.

$$-2u \leq n \leq 2u \tag{A.4}$$

If $0 < u < 1/2$, the relation $-1 < n < 1$ is obtained and n does not exist. Therefore, there is no such ξ', i.e., there is no ambiguities.

If $u = 1/2$, the relation $-1 \leq n \leq 1$ is obtained and $n = \pm 1$ satisfies the relation. When $n = \pm 1$, the relation $\xi' = \xi \mp 2$ is obtained from Eq. A.3. Therefore, the ambiguity occurs when the signal comes from the direction $\xi = \pm 1$. There is no ambiguity except for the directions mentioned above.

When $u > 1/2$, n exists which satisfies Eq. A.4 since $2u > 1$. Therefore, the ambiguities exist and the ambiguity interval is $1/u$ from Eq. A.3.

The same is true for linear arrays with element spacing $d = [0, v, 0]$. When $w = 0$, u and v (ξ and η) are independent in Eq. A.1. Therefore, the same is true even for two-dimensional arrays.

Appendix B

Mutual Coupling

The mutual coupling effect is an effect in which the output current of the antennas differs from the theoretical values when the antennas are close to each other, due to the mutual exchange of energy by rescattering [24][25][26][27][28][29][30][31][32][2]. It depends on the antenna characteristics and the antenna spacing, and the closer the antenna spacing, the greater the effect.

Figure B.1a shows the coupling paths between antennas m and n in the transmitting mode, in which the antenna element n is excited by a source, while antenna element m is not transmitting (passive). The energy generated at the source travels the complex paths as shown in the figure. Figure B.1b shows the coupling paths between antennas m and n in the receiving mode, in which the incident wave comes from free space. The energy of the incident wave travels the complex paths as well. This thesis focuses only on the receiving mode.

Consider that an arbitrary N-element antenna array receives one incident wave from an arbitrary direction. The coupled terminal voltage V_n at the element n can be expressed as

$$V_n = Z_L I_n = U_n + W_n \tag{B.1}$$

where Z_L is the load impedance, I_n is the current, U_n is the theoretical terminal voltage, and W_n is the voltage due to the mutual coupling efffect. W_n can be written as

$$W_n = Z_t^{n,1} I_1 + \cdots + Z_t^{n,n-1} I_{n-1} + Z_t^{n,n+1} I_{n+1} + \cdots Z_t^{n,N} I_N \tag{B.2}$$

where $Z_t^{n,i}$ is the receiving mutual impedance between antenna n and i, and I_i is the current induced at the terminal of the element i. Therefore, the relation between V_n and U_n can be expressed as

$$\begin{bmatrix} 1 & -\frac{Z_t^{1,2}}{Z_L} & \cdots & -\frac{Z_t^{1,N-1}}{Z_L} & -\frac{Z_t^{1,N}}{Z_L} \\ -\frac{Z_t^{2,1}}{Z_L} & 1 & \cdots & -\frac{Z_t^{2,N-1}}{Z_L} & -\frac{Z_t^{2,N}}{Z_L} \\ \vdots & \vdots & \ddots & \vdots & \vdots \\ -\frac{Z_t^{N-1,1}}{Z_L} & -\frac{Z_t^{N-1,2}}{Z_L} & \cdots & 1 & -\frac{Z_t^{N-1,N}}{Z_L} \\ -\frac{Z_t^{N,1}}{Z_L} & -\frac{Z_t^{N,2}}{Z_L} & \cdots & -\frac{Z_t^{N,N-1}}{Z_L} & 1 \end{bmatrix} \begin{bmatrix} V_1 \\ V_2 \\ \vdots \\ V_{N-1} \\ V_N \end{bmatrix} = \begin{bmatrix} U_1 \\ U_2 \\ \vdots \\ U_{N-1} \\ U_N \end{bmatrix} \tag{B.3}$$

It can be expressed simply as the following:

$$C\boldsymbol{v} = \boldsymbol{u} \tag{B.4}$$

where C is the $N \times N$ transformation matrix indicating the mutual coupling effect.

The more simple model for the mutual coupling effect is to represent C as follows [26][34]

$$c_{m,n} = \begin{cases} c d_{m,n} & \text{if} \quad d_{m,n} \leq B \\ 0 & \text{otherwise} \end{cases} \tag{B.5}$$

where $c_{m,n}$ is the (m,n) element of the matrix C, $d_{m,n}$ is the spacing between the element m and n, and c and B are the parameters. The simulations in 2.4 use this model to represent the mutual coupling effect.

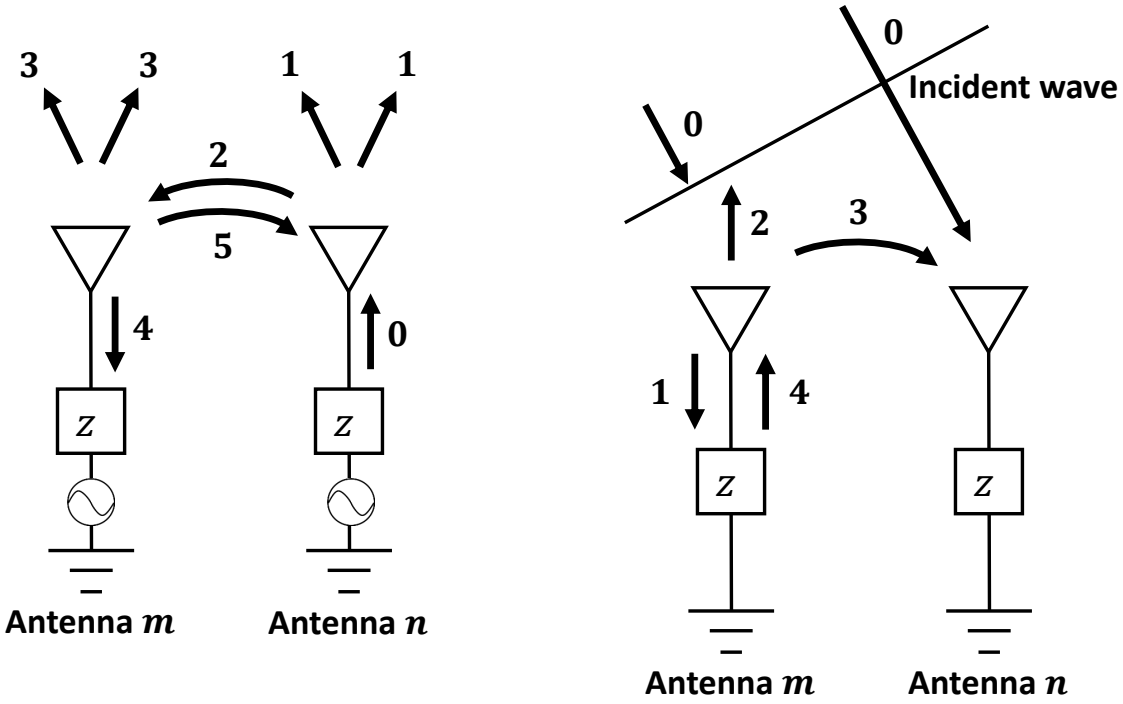

(a) Transmitting mode. (b) Receiving mode.

Fig. B.1: Coupling paths between antennas m and n [2].

By estimating C, the theoretical voltage can be obtained from the coupled voltage. One of the method of estimating C is to measure the coupled voltages induced by the incident waves from the distinct directions and to apply the least squares method. If the coupled voltages induced by the incident waves from L distinct directions are measured, C can be estimated by the applying least squares method to the following relation

$$CV = U \tag{B.6}$$

$$V = \left[\boldsymbol{v}_1 \cdots \boldsymbol{v}_L\right] \tag{B.7}$$

$$U = \left[\boldsymbol{u}_1 \cdots \boldsymbol{u}_L\right] \tag{B.8}$$

where $\boldsymbol{v}_i$ and $\boldsymbol{u}_i$ is the coupled and theoretical voltage vectors when the incident wave comes from i-th direction. This thesis uses this method to estimate the transformation matrix in the DOA estimation experiment (**??**).

Appendix C

Cramér-Rao Low Boundary

Cramér-Rao low bound (CRLB) [35][36] is defined as the lower bound for the variance of an unbiased estimator of the unknown population of a given probability distribution. The correlation matrix is expressed as follows (same as Eq. 2.24):

$$R = ASA^H + P_{noise}I \tag{C.1}$$

The CRLB for DOA estimation [37][38] is given by

$$CRLB_\omega = \frac{P_{noise}}{2L}\{\mathrm{Re}[(A_\omega^H \Pi_A^\perp A_\omega) \odot (SA^H R^{-1} AS)^T]\}^{-1} \qquad (\omega = \xi, \eta) \tag{C.2}$$

$$A_\omega = \begin{bmatrix} \frac{\partial \boldsymbol{a}_1}{\partial \omega_1} & \frac{\partial \boldsymbol{a}_2}{\partial \omega_2} & \cdots & \frac{\partial \boldsymbol{a}_N}{\partial \omega_N} \end{bmatrix} \tag{C.3}$$

$$\Pi_A^\perp = I - A(A^H A)^{-1} A^H \tag{C.4}$$

, where L is the number of snapshots and $\odot$ is the Hadamard product. CRLB is determined solely by SNR, the number of snapshots, array arrangement and DOAs. Therefore, the lower bound of the estimation error variance can be obtained analytically, independent of the estimation algorithm. The CRLB allows the performance of the array placement to be evaluated.

The relation between CRLB and variance of MUSIC σ_{MUSIC,ω_i} [39] is expressed as follows:

$$\frac{\sigma^2_{MUSIC,\omega_i}}{CRLB_{\omega_i}} = 1 + \frac{[(A^H A)^{-1}]_{ii}}{SNR_i} \tag{C.5}$$

, where $[\ \ ]_{ii}$ is the (i,i) element of the matrix. Therefore, the variance of MUSIC is estimated analytically using the CRLB.

Appendix D

DOA Estimation Algorithm

DOA estimation method uses the cross-correlation matrix obtained by the array antennas to estimate the direction of the signal source. Various algorithms have been proposed.

D.1 FFT

Although fast Fourier transfer (FFT) method is not generally classified as a DOA estimation method, it is the most basic method of knowing the direction of a radio source. By performing a two-dimensional inverse Fourier transform on the cross-correlation (visibility) $\mathcal{V}(u, v)$ obtained for any baseline vector, the signal intensity distribution $I(\xi, \eta)$ can be obtained.

$$I(\xi, \eta) = \int \int_{u,v} \mathcal{V}(u, v) \exp\left[2\pi i(u\xi + v\eta)\right] du dv \tag{D.1}$$

In practical use, the intensity distribution $I(\xi, \eta)$ is obtained by using a 2D inverse FFT on the obtained visibility. If the visibility $\mathcal{V}$ is obtained at the baseline $[u_j, v_k](j = 1, \cdots, m, k = 1, \cdots, n)$, the signal intensity $\hat{I}$ is calculate as follows:

$$\hat{I}(\xi, \eta) = \frac{1}{m} \sum_{j=1}^{m} \frac{1}{n} \sum_{k=1}^{n} \mathcal{V}(u_j, v_k) \exp\left[2\pi i \frac{u_j}{m} \xi\right] \exp\left[2\pi i \frac{v_k}{n} \eta\right] \tag{D.2}$$

Ideally, visibility should be obtained on all baselines, but it is difficult to achieve it in practice. Because some of the visibility samples are not obtained, the estimated signal intensity differs from the true one. In addition, the resolution is limited by the array beamwidth.

D.2 Beamformer

Beamformer is one of the most basic DOA estimation methods [19]. Scan the main beam of the array antenna in all directions to determine the direction with the highest output power. The scan is performed by adjusting the phase with weights in the channel of each antenna element. When the main beam of the array antenna is pointed at (ξ, η), the weight vector is obtained as follows:

$$\boldsymbol{w}(\xi, \eta) = [w_1, \cdots, w_M] \tag{D.3}$$

$$w_m = \exp\left[j \frac{2\pi}{\lambda} \hat{\boldsymbol{r}}_m^T \hat{\boldsymbol{L}}(\xi, \eta)\right] \tag{D.4}$$

Then the output power of the array is expressed as

$$P_{out}(\xi, \eta) = \frac{1}{2} \boldsymbol{w}^H(\xi, \eta) R_{xx} \boldsymbol{w}(\xi, \eta) \tag{D.5}$$

The angular spectrum can be expressed by normalizing the output power:

$$P_{BF}(\xi,\eta) = \frac{\boldsymbol{w}^H(\xi,\eta) R_{xx} \boldsymbol{w}(\xi,\eta)}{\boldsymbol{w}^H(\xi,\eta)\boldsymbol{w}(\xi,\eta)} \tag{D.6}$$

Thus, the DOA can be estimated from the peak of P_{BF}. However, its angular resolution is low, constrained by the main beam width.

D.3 Algorithms using Eigen-decomposition of R_{xx}

Some algorithms achieve higher angular resolution than Beamformer by utilizing an eigenvalue decomposition of the cross-correlation matrix. If there is no noise power (i.e. $P_{noise} = 0$), the cross-correlation matrix R_{xx} is eigen-decomposed as follows:

$$ASA^H \boldsymbol{e}_i = \mu_i \boldsymbol{e}_i \qquad (i = 1, 2, \cdots, M) \tag{D.7}$$

where μ_i is the eigenvalue and $\boldsymbol{e}_i$ is the eigenvector associated with μ_i. Each of the eigenvalues has the following major and minor relationships:

$$\mu_1 \geq \mu_2 \geq \cdots \geq \mu_N \geq \mu_{N+1} = \cdots = \mu_M = 0 \tag{D.8}$$

If there is noise power (i.e. $P_{noise} \neq 0$), the eigen-decomposition of R_{xx} is expressed as follows:

$$(ASA^H + P_{noise} I)\boldsymbol{e}_i = ASA^H \boldsymbol{e}_i + P_{noise}\boldsymbol{e}_i = (\mu_i + P_{noise})\boldsymbol{e}_i \tag{D.9}$$

If λ_i is defined as $\lambda \equiv \mu_i + P_{noise}$, it represent the eigen value of R_{xx}. Their relations are as follows:

$$\lambda_1 \geq \lambda_2 \geq \cdots \geq \lambda_N \geq \lambda_{N+1} = \cdots = \lambda_M = P_{noise} \tag{D.10}$$

Comparing Eqs. (D.8) and (D.10), it can be said that:

- $\lambda_i \quad (i = N+1, \cdots, M)$ is equivalent to the noise power.
- $\lambda_i \quad (i = 1, \cdots, N)$ is related to the signal power.
- $\boldsymbol{e}_i \quad (i = 1, \cdots, M)$ is not changed by the noise power.
- Since the eigen vectors are orthogonal to each other, they are the orthonormal basis vector of the Hermitian space of dimension M. This space is divided into the following two subspaces:

$$\mathcal{S} = span\{\boldsymbol{e}_1, \boldsymbol{e}_2, \cdots, \boldsymbol{e}_N\} \tag{D.11}$$

$$\mathcal{N} = span\{\boldsymbol{e}_{N+1}, \boldsymbol{e}_{N+2}, \cdots, \boldsymbol{e}_M\} \tag{D.12}$$

  $\mathcal{S}$ is called as *signal subspace* and $\mathcal{N}$ is called as *noise subspace*.

D.3.1 MUSIC

MUSIC (MUltiple SIgnal Classification) [20] focuses on the noise subspace of the two subspaces. The MUSIC spectrum is expressed as follows:

$$P_{MU}(\xi,\eta) = \frac{\boldsymbol{a}^H(\xi,\eta)\boldsymbol{a}(\xi,\eta)}{\boldsymbol{a}^H(\xi,\eta) E_N E_N^H \boldsymbol{a}(\xi,\eta)} \tag{D.13}$$

Its peaks are regarded as the DOAs. The estimation error covariance for MUSIC is calculated analytically using Eq. C.5. Since spectral search is required, the computational cost is relatively high. Furthermore, the estimation accuracy depends on the fineness of the spectral search. However, it can be applied to arbitrary array configurations.

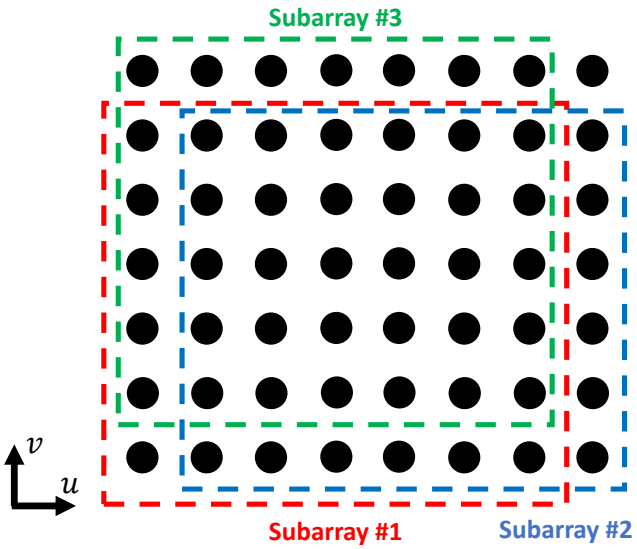

Fig. D.1: Subarrays for ESPRIT.

D.3.2 ESPRIT

ESPRIT (Estimation of Signal Parameters via Rotational Invariance Techniques) [21] requires the use of two identical array antennas. They are called subarrays and overlap perfectly when one is displaced by $\mathbf{\Delta}$. To satisfy this condition, the arrays should be uniformly arranged, such as URA. However, arrays such as hole-free sparse arrays, in which differential coarrays are equivalent to URAs, can be treated as equivalent to URAs.

As shown in Fig. D.1, there are $M \times N$ URAs and three $(M-1) \times (N-1)$ subarrays are considered. First, the two subarrays #1 and #2 are considered. The phase difference on l-th signal can be expressed as

$$\phi_l = 2\pi \Delta_u \xi_l \tag{D.14}$$

As shown in Eq. 2.18, the received signal at each subarray can be expressed as follows:

$$\boldsymbol{X}_1(t) = A_1 \boldsymbol{F}(t) + \mathbf{\Sigma}_1(t) \tag{D.15}$$

$$\boldsymbol{X}_2(t) = A_2 \boldsymbol{F}(t) + \mathbf{\Sigma}_2(t) \tag{D.16}$$

$$A_2 = A_1 \Phi \tag{D.17}$$

$$\Phi = \mathrm{diag}[e^{j\phi_1}, e^{j\phi_2}, \cdots, e^{j\phi_N}] \tag{D.18}$$

$$J_1 A \Phi = J_2 A \tag{D.19}$$

$$J_1 = \begin{bmatrix} 1 & 0 & 0 & \cdots & 0 & 0 \\ 0 & 1 & 0 & & & 0 \\ \vdots & \vdots & \vdots & \vdots & \vdots & \vdots \\ 0 & \cdots & \cdots & 0 & 1 & 0 \end{bmatrix} \tag{D.20}$$

$$J_2 = \begin{bmatrix} 0 & 1 & 0 & \cdots & 0 & 0 \\ 0 & 0 & 1 & & & 0 \\ \vdots & \vdots & \vdots & \vdots & \vdots & \vdots \\ 0 & \cdots & \cdots & 0 & 0 & 1 \end{bmatrix} \tag{D.21}$$

The L-dimensional subspace stretched by the L vectors that make up A is the signal subspace and coincides with the subspace of $\{\boldsymbol{e}_1, \boldsymbol{e}_2, \cdots, \boldsymbol{e}_L\}$.

$$E_S = AT \tag{D.22}$$

, where $E_S = [\boldsymbol{e}_1, \boldsymbol{e}_2, \cdots, \boldsymbol{e}_L]$ and T is a regular matrix.

$$J_2 E_S T^{-1} = J_1 E_S T^{-1} \Phi \Leftrightarrow J_2 E_S = J_1 E_S T^{-1} \Phi T \tag{D.23}$$

If Ψ is defined as $\Psi \equiv T^{-1}\Phi T$, Φ and T is the eigenvalue matrix and the eigenvector matrix of Ψ. Equation D.23 becomes as follows:

$$J_2 E_S = J_1 E_S \Psi \tag{D.24}$$

After obtaining Ψ by the least squares method, its eigenvalues and eigenvectors are obtained. The eigenvalues are the diagonal component $\exp j\phi_l$ of Φ, and the DOA ξ_l can be obtained.

Next, the subarrays #1 and #3 are considered. Subarrays #1 and #3 can be considered in the same way as #1 and #2. The phase difference on l-th signal can be expressed as

$$\phi_l = 2\pi \Delta_v \eta_l \tag{D.25}$$

and η_l can be obtained by the eigen-decomposition of Ψ. The direction of the signal source can be estimated based on the above procedures.

Unitary ESPRIT

Unitary ESPRIT [22][23] performs a real number operation by placing the phase center at the center of the array, which enhances computational efficiency. This thesis employs Unitary ESPRIT instead of ESPRIT in the simulations.

Bibliography

[1] Japan Aerospace Exploration Agancy. Japan's scenario for international space exploration. Japan Aerospace Exploration Agancy, 2021. EZA-2021002.

[2] Constantine A. Balanis. *Antenna Theory: Analysis and Design*. Wiley-Interscience, 4 edition, 2016.

[3] Takanao Saiki, Yuichi Tsuda, Osamu Mori, Yuri Shimaki, Yusuke Maru, Yuto Takei, Hirotaka Sawada, Hiroki Nakanishi, Yuya Mimasu, Shota Kikuchi, Yuki Takao, Ahmed Kiyoshi Sugihara, Kazuhiko Yamada, Ryu Funase, and Junji Kikuchi. Engineering study status of next generation small body sample return mission. In *23rd Space Science Symposium*, 2023.

[4] Shuichi Sato, Seiji Kawamura, Masaki Ando, Takashi Nakamura, Kimio Tsubono, Akito Araya, Ikkoh Funaki, Kunihito Ioka, Nobuyuki Kanda, Shigenori Moriwaki, Mitsuru Musha, Kazuhiro Nakazawa, Kenji Numata, Shin ichiro Sakai, Naoki Seto, Takeshi Takashima, Takahiro Tanaka, Kazuhiro Agatsuma, Koh suke Aoyanagi, Koji Arai, Hideki Asada, Yoichi Aso, Takeshi Chiba, Toshikazu Ebisuzaki, Yumiko Ejiri, Motohiro Enoki, Yoshiharu Eriguchi, Masa-Katsu Fujimoto, Ryuichi Fujita, Mitsuhiro Fukushima, Toshifumi Futamase, Katsuhiko Ganzu, Tomohiro Harada, Tatsuaki Hashimoto, Kazuhiro Hayama, Wataru Hikida, Yoshiaki Himemoto, Hisashi Hirabayashi, Takashi Hiramatsu, Feng-Lei Hong, Hideyuki Horisawa, Mizuhiko Hosokawa, Kiyotomo Ichiki, Takeshi Ikegami, Kaiki T. Inoue, Koji Ishidoshiro, Hideki Ishihara, Takehiko Ishikawa, Hideharu Ishizaki, Hiroyuki Ito, Yousuke Itoh, Nobuki Kawashima, Fumiko Kawazoe, Naoko Kishimoto, Kenta Kiuchi, Shiho Kobayashi, Kazunori Kohri, Hiroyuki Koizumi, Yasufumi Kojima, Keiko Kokeyama, Wataru Kokuyama, Kei Kotake, Yoshihide Kozai, Hideaki Kudoh, Hiroo Kunimori, Hitoshi Kuninaka, Kazuaki Kuroda, Kei ichi Maeda, Hideo Matsuhara, Yasushi Mino, Osamu Miyakawa, Shinji Miyoki, Mutsuko Y. Morimoto, Tomoko Morioka, Toshiyuki Morisawa, Shinji Mukohyama, Shigeo Nagano, Isao Naito, Kouji Nakamura, Hiroyuki Nakano, Kenichi Nakao, Shinichi Nakasuka, Yoshinori Nakayama, Erina Nishida, Kazutaka Nishiyama, Atsushi Nishizawa, Yoshito Niwa, Taiga Noumi, Yoshiyuki Obuchi, Masatake Ohashi, Naoko Ohishi, Masashi Ohkawa, Norio Okada, Kouji Onozato, Kenichi Oohara, Norichika Sago, Motoyuki Saijo, Masaaki Sakagami, Shihori Sakata, Misao Sasaki, Takashi Sato, Masaru Shibata, Hisaaki Shinkai, Kentaro Somiya, Hajime Sotani, Naoshi Sugiyama, Yudai Suwa, Rieko Suzuki, Hideyuki Tagoshi, Fuminobu Takahashi, Kakeru Takahashi, Keitaro Takahashi, Ryutaro Takahashi, Ryuichi Takahashi, Tadayuki Takahashi, Hirotaka Takahashi, Takamori Akiteru, Tadashi Takano, Keisuke Taniguchi, Atsushi Taruya, Hiroyuki Tashiro, Yasuo Torii, Morio Toyoshima, Shinji Tsujikawa, Yoshiki Tsunesada, Akitoshi Ueda, Ken ichi Ueda, Masayoshi Utashima, Yaka Wakabayashi, Hiroshi Yamakawa, Kazuhiro Yamamoto, Toshitaka Yamazaki, Jun'ichi Yokoyama, Chul-Moon Yoo, Shijun Yoshida, and Taizoh Yoshino. The status of DECIGO. *Journal of Physics: Conference Series*, 840(1):012010, may 2017.

[5] Karsten Danzmann and Albrecht Rüdiger. LISA technology—concept, status, prospects. *Classical and Quantum Gravity*, 20(10):S1, apr 2003.

[6] Marshall Smith, Douglas Craig, Nicole Herrmann, Erin Mahoney, Jonathan Krezel, Nate McIntyre, and Kandyce Goodliff. The Artemis program: An overview of NASA's activities to return humans to the Moon. In *2020 IEEE Aerospace Conference*, pages 1–10, 2020.

[7] Brian K. Muirhead, Austin Nicholas, and Jeff Umland. Mars sample return mission concept status. In *2020 IEEE Aerospace Conference*, pages 1–8, 2020.

[8] Jacqueline Le Moigne, Michael M. Little, and Marjorie C. Cole. New Observing Strategy (NOS) for future earth science missions. In *IGARSS 2019 - 2019 IEEE International Geoscience and Remote Sensing Symposium*, pages 5285–5288, 2019.

[9] Hugo Carreno-Luengo, Juan A. Crespo, Ruzbeh Akbar, Alexandra Bringer, April Warnock, Mary Morris, and Chris Ruf. The CYGNSS mission: On-going science team investigations. *Remote Sensing*, 13(9), 2021.

[10] Sei-Ichiro Watanabe, Yuichi Tsuda, Makoto Yoshikawa, Satoshi Tanaka, Takanao Saiki, Satoru Nakazawa, and B S Watanabe. Hayabusa2 mission overview. *Space Sci Rev*, 208:3–16, 2017.

[11] Stefano Campagnola, Chit Hong Yam, Yuichi Tsuda, Naoko Ogawa, and Yasuhiro Kawakatsu. Mission analysis for the martian moons explorer (MMX) mission. *Acta Astronautica*, 146:409–417, 2018.

[12] Zachary Manchester, Mason Peck, and Andrew Filo. Kicksat: A crowd-funded mission to demonstrate the world' s smallest spacecraft. 2013.

[13] Takahide Mizuno, T Kase, T Shiina, Makoto Mita, Noriyuki Namiki, Hiroki Senshu, Ryuhei Yamada, Hirotomo Noda, Hiroo Kunimori, Naru Hirata, et al. Development of the laser altimeter (LIDAR) for Hayabusa2. *Space Science Reviews*, 208:33–47, 2017.

[14] Takahiro Sasaki, Moeko Hidaka, Yuki Tomita, Yuri Hachiya, Yoshinori Kondo, Ryo Nakamura, and Toru Yamamoto. Proximity operation and automated docking on HTV-X: Guidance, navigation, and control strategy. In *2022 IEEE Aerospace Conference (AERO)*, pages 1–10, 2022.

[15] Timothy P. Setterfield, Robert A. Hewitt, Po-Ting Chen, Antonio Terán Espinoza, Nikolas Trawny, and Anup Katake. LiDAR-inertial based navigation and mapping for precision landing. In *2021 IEEE Aerospace Conference (50100)*, pages 1–19, 2021.

[16] Satoshi Ueda, Toru Kasai, and Hirohiko Uematsu. HTV rendezvous technique and GN&C design evaluation based on 1st flight on-orbit operation result. In *AIAA/AAS Astrodynamics Specialist Conference*, page 7664, 2010.

[17] G. Gaias, S. D' Amico, and J.-S. Ardaens. Angles-only navigation to a noncooperative satellite using relative orbital elements. *Journal of Guidance, Control, and Dynamics*, 37(2):439–451, 2014.

[18] Jean-Sébastien Ardaens and Gabriella Gaias. Angles-only relative orbit determination in low earth orbit. *Advances in Space Research*, 61(11):2740–2760, 2018.

[19] Nobuyoshi Kikuma. *Adaptive signal processing by array an-tennas.* Kagaku-Gijutsu-Shuppan, 1998.

[20] Ralph O. Schmidt. Multiple emitter location and signal parameter estimation. *IEEE Transactions on Antennas and Propagation*, AP-34:276–280, 1986.

[21] Richard Roy and Thomas Kailath. Esprit—estimation of signal parameters via rotational invariance techniques. *IEEE Transactions on Acoustics, Speech, and Signal Processing*, 37:984–995, 1989.

[22] M. Haardt and J.A. Nossek. Unitary esprit: how to obtain increased estimation accuracy with a reduced computational burden. *IEEE Transactions on Signal Processing*, 43(5):1232–1242, 1995.

[23] Michael D Zoltowski, Martin Haardt, and Cherian P Mathews. Closed-form 2-d angle estimation with rectangular arrays in element space or beamspace via unitary esprit. *IEEE Transactions on Signal Processing*, 44:316–328, 1996.

[24] Inder J. Gupta and Aharon A. Ksienski. Effect of mutual coupling on the performance of adaptive arrays. *IEEE Transactions on Antennas and Propagation*, 31:785–791, 1983.

[25] Hans Steyskal and Jeffrey S. Herd. Mutual coupling compensation in small array antennas. *IEEE Transactions on Antennas and Propagation*, 38:1971–1975, 1990.

[26] Benjamin Friedlander and Anthony J. Weiss. Direction finding in the presence of mutual coupling. *IEEE Transactions on Antennas and Propagation*, 39:273–284, 1991.

[27] Charles Shipley and Don Woods. Mutual coupling-based calibration of phased array antennas. pages 529–532. IEEE, 2000.

[28] Tao Su and Hao Ling. On modeling mutual coupling in antenna arrays using the coupling matrix. *Microwave and Optical Technology Letters*, 28:231–237, 2 2001.

[29] H. T. Hui. A new definition of mutual impedance for application in dipole receiving antenna arrays. *IEEE Antennas and Wireless Propagation Letters*, 3:364–367, 12 2004.

[30] Hoi-Shun Lui, Hon Tat Hui, and Mook Seng Leong. A note on the mutual-coupling problems in transmitting and receiving antenna arrays. *IEEE Antennas and Propagation Magazine*, 51(5):171–176, 2009.

[31] Shogo Nakamura and Koichi Ichige. An optimum 2d sparse array configuration with reduced mutual coupling; an optimum 2d sparse array configuration with reduced mutual coupling. *2018 International Symposium on Antennas and Propagation (ISAP)*, 2018.

[32] T. T. Vo, L. Ouvry, A. Sibille, and S. Bories. Mutual coupling modeling and calibration in antenna arrays for aoa estimation. *2018 2nd URSI Atlantic Radio Science Meeting (AT-RASC)*, pages 1–4, 2018.

[33] Chun-Lin Liu and P. P. Vaidyanathan. Two-dimensional sparse arrays with hole-free coarray and reduced mutual coupling. In *2016 50th Asilomar Conference on Signals, Systems and Computers*, pages 1508–1512, 2016.

[34] Chun Lin Liu and Palghat P. Vaidyanathan. Hourglass arrays and other novel 2-d sparse arrays with reduced mutual coupling. *IEEE Transactions on Signal Processing*, 65:3369–3383, 7 2017.

[35] Harald Cramér. *Mathematical methods of statistics*, volume 26. Princeton university press, 1999.

[36] C. Radhakrishna Rao. *Information and the Accuracy Attainable in the Estimation of Statistical Parameters*, pages 235–247. Springer New York, New York, NY, 1992.

[37] Petre Stoica and Randolph Moses. *Spectral analysis of signals*, volume 452. Pearson Prentice Hall Upper Saddle River, NJ, 2005.

[38] P. Stoica, E.G. Larsson, and A.B. Gershman. The stochastic CRB for array processing: a textbook derivation. *IEEE Signal Processing Letters*, 8(5):148–150, 2001.

[39] Petre Stoica and Arye Nehorai. MUSIC, maximum likelihood, and Cramér-Rao bound. *IEEE Transactions on Acoustics, Speech, and Signal Processing*, 37:720–741, 1989.